Focus Section: Data Mine: 2019 Ridgecrest, California Earthquake Sequence

Survey and Continuous GNSS in the Vicinity of the July 2019 Ridgecrest Earthquakes

Michael Floyd[*1], Gareth Funning[2], Yuri Fialko[3], Rachel Terry[2,4], and Thomas Herring[1]

Abstract

The M_w 6.4 and M_w 7.1 Ridgecrest, California, earthquakes of July 2019 occurred within 34 hr of each other on conjugate strike-slip faults in the Mojave Desert, just north of the central Garlock fault. Here, we present the results of a survey of 18 Global Navigation Satellite Systems (GNSS) sites conducted in the immediate aftermath of the earthquakes, including five sites that recorded the motion of the second earthquake after having been set up immediately following the first, as well as processed results from continuous GNSS sites throughout the region. Our field work in response to the earthquakes provides additional constraints on the ground displacement due to both earthquakes, complementing data from a spatially sparser network of continuously recording GNSS sites in the area, as well as temporally sparser Interferometric Synthetic Aperture Radar data that were able to capture a combined deformation signal from the two earthquakes.

Cite this article as Floyd, M., G. Funning, Y. Fialko, R. Terry, and T. Herring (2020). Survey and Continuous GNSS in the Vicinity of the July 2019 Ridgecrest Earthquakes, *Seismol. Res. Lett.* **XX**, 1–8, doi: 10.1785/0220190324.

Supplemental Material

Introduction

The pair of large earthquakes near Ridgecrest, California, in July 2019—an M_w 6.4 event on 4 July and an M_w 7.1 event on 5 July, local time (6 July, Universal Time)—occurred 34 hr apart in a region with a number of geodetic monuments with many years of archived Global Navigation Satellite Systems (GNSS), specifically Global Positioning System (GPS), survey data. The earthquakes occurred on conjugate faults in a region of active deformation and seismicity in the eastern California shear zone (ECSZ), and in proximity to the Coso geothermal field and to the Garlock fault, both of which had been targets for study in these earlier GNSS surveys, in the 1990s and early 2000s (e.g., McClusky *et al.*, 2001; Miller, Johnson, *et al.*, 2001; Fig. 1 and Table 1).

In more recent years, some of these survey sites were reoccupied with GNSS equipment to improve uncertainties of the secular velocities at those sites (e.g., Funning, Terry, and Floyd, 2019). These recent surveys, and the knowledge gained from them, facilitated a rapid response to the first Ridgecrest earthquake (and therefore to the second earthquake as well), enabling the separation of the coseismic displacements of the two events. Additional, and ongoing, survey measurements made in the days following the second M_w 7.1 earthquake will enable the study of postseismic deformation due to the Ridgecrest events. When combined with data from continuous GNSS stations in the region, the Network of the Americas (NOTA) operated as part of the Geodesy Advancing Geoscience and EarthScope (GAGE) facility at UNAVCO, and stations operated by the U.S. Geological Survey (USGS), a detailed picture of the Ridgecrest events and their aftermath is provided. In contrast to Interferometric Synthetic Aperture Radar measurements of the coseismic displacements, which can only constrain the total displacement from the two earthquakes and the first few days of postseismic response (e.g., Wang and Bürgmann, 2019; Xu and Sandwell, 2019), the available GNSS data can measure coseismic displacements due to the M_w 6.4 and M_w 7.1 events individually, as well as separate coseismic signals from any postseismic deformation. As such, they provide a useful resource for researchers interested in constraining models of coseismic slip or postseismic response, in addition to providing a foundation for potential future investigations regarding fault interactions and stress transfer.

In this study, we describe the archived survey data sets from the region and the survey response to the Ridgecrest earthquakes to present a combined solution from both survey and continuous GNSS sites for the displacements during the Ridgecrest earthquakes.

1. Department of Earth, Atmospheric and Planetary Sciences, Massachusetts Institute of Technology, Cambridge, Massachusetts, U.S.A.; 2. Department of Earth Sciences, University of California, Riverside, Riverside, California, U.S.A.; 3. Institute of Geophysics and Planetary Physics, Scripps Institution of Oceanography, University of California, San Diego, La Jolla, California, U.S.A.; 4. Now at UNAVCO, Boulder, Colorado, U.S.A.

*Corresponding author: mfloyd@mit.edu

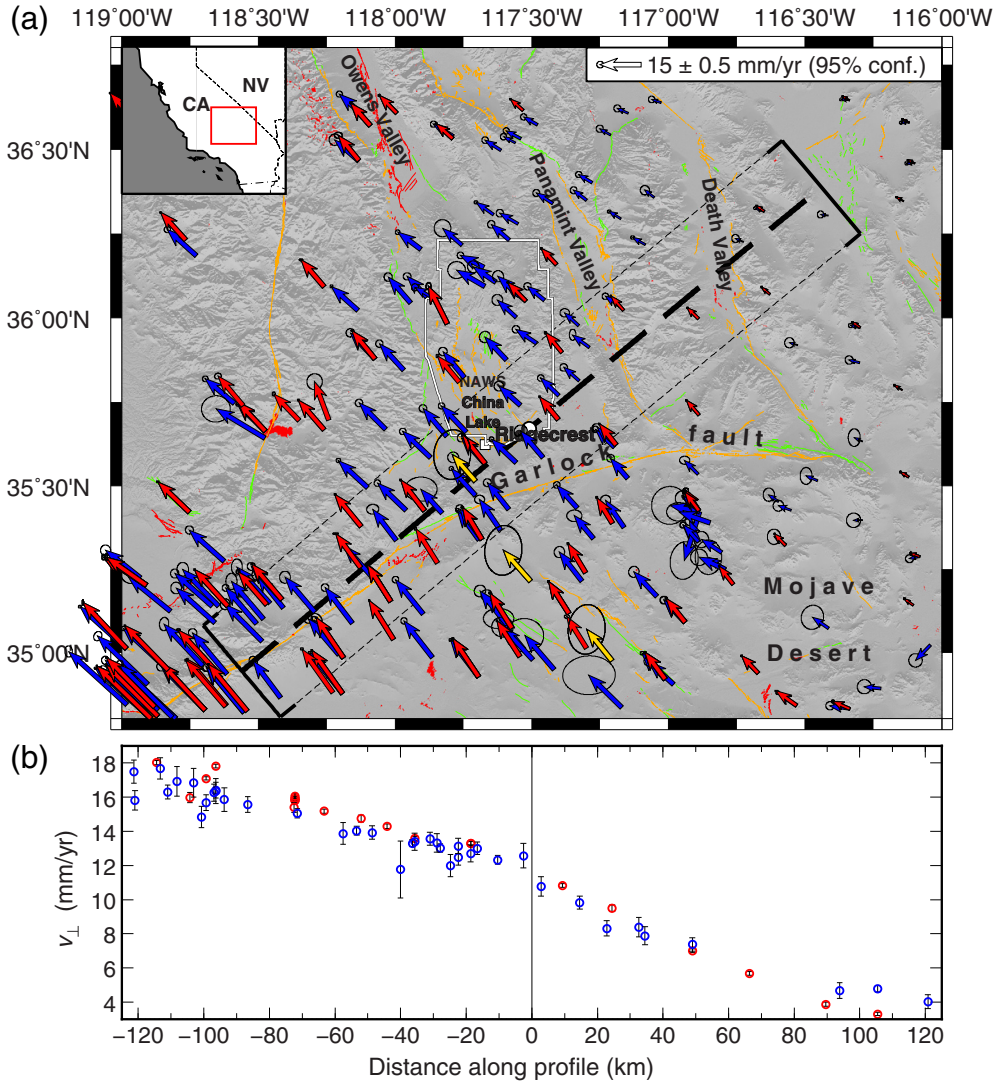

Figure 1. (a) Global Navigation Satellite Systems velocity solution, relative to North America (Altamimi *et al.*, 2017), across the Mojave Desert region from Geodesy Advancing Geoscience and EarthScope products for continuous sites (red; Herring *et al.*, 2016), Southern California Earthquake Center's (SCEC's) Crustal Motion Map for survey sites (blue; Shen *et al.*, 2011, rotated from their Stable North America Reference Frame, SNARF, to the same Altamimi *et al.*, 2017, definition of North America), and updated or new velocities for sites observed since by Funning (2016) and Funning, Terry, and Floyd (2019) within our region of interest (yellow; this study). Orange and green lines are mapped faults with evidence of displacement during the last 15 and 130 ky, respectively, from the U.S. Geological Survey (USGS) Quaternary Fault and Fold Database (USGS and California Geological Survey, 2006). The white line is the boundary of the Naval Air Weapons Station (NAWS) China Lake. (b) The profile, centered at the intersection of the M_w 6.4 and M_w 7.1 surface ruptures, shows the velocity gradient (mostly profile-perpendicular, i.e., fault-parallel, shear) across the region. The color version of this figure is available only in the electronic edition.

Previous Surveys and Velocity Solutions

Surveys throughout the Mojave Desert in the region of the Garlock fault were conducted mostly in the 1990s and early 2000s (see Table 1). These focused on two aspects of the region, the relative motion of faults, including the Garlock fault, throughout the ECSZ from the California–Nevada state line in the northeast to the San Andreas fault in the southwest, and the deformation of the Coso geothermal field where the geothermal energy production is associated with subsidence at a rate of a few centimeters per year (e.g., Fialko and Simons, 2000; Tymofyeyeva and Fialko, 2015). The GNSS survey results related to the former were presented by Miller, Johnson, *et al.* (2001) and McClusky *et al.* (2001). The latter study inferred a strike-slip motion across the Airport Lake fault (the previously mapped fault most closely, although not exactly, associated with the M_w 7.1 Ridgecrest earthquake) to be 5.7 ± 0.7 mm/yr. Shen *et al.* (2011) presented a rigorous reprocessing and combination of surveys throughout California for the Southern California Earthquake Center (SCEC) Crustal Motion Map (Fig. 1; blue vectors and circles). The region also contains a network of continuously operating sites (Fig. 1; red vectors and circles), which are processed routinely, and derived products such as velocity solutions are generated and available publicly from UNAVCO (see Data and Resources). The continuous velocity solution shown in Figure 1 is that of Herring, Floyd, *et al.* (2018).

The profile shown in Figure 1b across this latest velocity solution shows a similar velocity gradient across the region, although we do not model it explicitly using elastic dislocations here to update the model of McClusky *et al.* (2001).

In more recent years, a group from the University of California, Riverside (UCR) conducted a survey in 2014 that mostly covered the southern and eastern Mojave Desert, as well as measuring a couple of sites further north in the Mojave, to the southwest of the July 2019 earthquakes (Funning, 2016). In addition to site occupations, the group conducted extensive site reconnaissance that was leveraged for later visits.

TABLE 1
Summary of Global Navigation Satellite Systems Surveys Used to Determine Pre-Earthquake Positions for This Study

Survey	Citation	DOI
Pre-earthquake velocity solution		
Mammoth/Mojave 1994	Miller *et al.* (1997)	10.7283/T57H1GGM
Mojave 1995	Miller *et al.* (1995)	10.7283/T5H12ZX8
Garlock 1997	Miller *et al.* (2001a)	10.7283/T55Q4T1H
Mojave 1997	Miller *et al.* (2001b)	10.7283/T5W66HPD
Garlock 1998 06 (Jun)	Miller *et al.* (2001c)	10.7283/T51Z4295
Mojave 1998 06 (Jun)	Miller *et al.* (2001d)	10.7283/T58G8HMF
Mojave 1998 12 (Dec)	Miller *et al.* (2001e)	10.7283/T50Z715S
Garlock 1998/1999	Miller *et al.* (2001f)	10.7283/T59G5JRT
Mojave 1999	Miller and Johnson (2001a)	10.7283/T56Q1V5W
Mojave 2000	Miller and Johnson (2001b)	10.7283/T5JW8BS7
Garlock 2000	Miller and Johnson (2001c)	10.7283/T5KW5CXM
Mojave 2001 03 (Mar)	Miller and Johnson (2001d)	10.7283/T5Z60KZ5
Garlock 2001 03 (Mar)	Miller and Johnson (2001e)	10.7283/T5TD9V79
Mojave 2001 06 (Jun)	Miller and Johnson (2001f)	10.7283/T5F769GJ
Garlock 2001 06 (Jun)	Miller and Johnson (2001g)	10.7283/T5G44N6M
GeoEarthScope 2005 (1)	Bevis and Hudnut (2005a)	10.7283/V5MV-QE58
GeoEarthScope 2005 (2)	Bevis and Hudnut (2005b)	10.7283/FQ3X-X311
San Jacinto Fault 2014	Funning (2016)	10.7283/T57H1GZW
Mojave 2019 (Feb)	Funning, Terry, and Floyd (2019)	10.7283/TFX5-EJ21
Mojave 2019 (Mar)	Funning, Terry, and Floyd (2019)	10.7283/TFX5-EJ21
Coseismic displacement solution		
Ridgecrest (UCSD)	Fialko *et al.* (2019a)	10.7283/N74Q-GA66
Post-Ridgecrest (UCSD)	Fialko *et al.* (2019b)	10.7283/YJK0-B215
Post-Ridgecrest (UCR)	Funning, Kyriakopoulos, *et al.* (2019)	10.7283/5ASB-9V26

UCR, University of California, Riverside; UCSD, University of California, San Diego.

The most recent pre-earthquake surveys were conducted in February and March 2019, again by a group from UCR (Funning, Terry, and Floyd, 2019). As part of a project funded by SCEC to update deformation velocities in the Mojave Desert region, 21 sites were occupied for durations of between 17 and 26 hr each (Fig. S1, available in the supplemental material to this article), including a transect of the Garlock fault southwest of Ridgecrest.

Survey Response to the July 2019 Earthquakes

A field team from UCR responded promptly to the 4 July event, arriving in the field that afternoon. On the afternoon of 4 July and morning of 5 July, we occupied four sites to the west and southwest of the epicenter (H701, J701, F048, and ATOL) that had previously been measured in February 2019, as well as one site to the south (PNCL) that had been measured in 2001. The first of these measurements were started within 7 hr of the M_w 6.4 earthquake, with all five sites within 32 km of the rupture operating within 26 hr (see Fig. S2). All five remained standing and running during and after the second M_w 7.1 earthquake that occurred 34 hr after the M_w 6.4, providing a unique, near-field constraint on the deformation from each event separately; as we will show later, site PNCL, fortuitously located only 600 m from the surface rupture of the M_w 7.1 event, detected the highest displacements—over 80 cm of horizontal displacement in the M_w 7.1 earthquake.

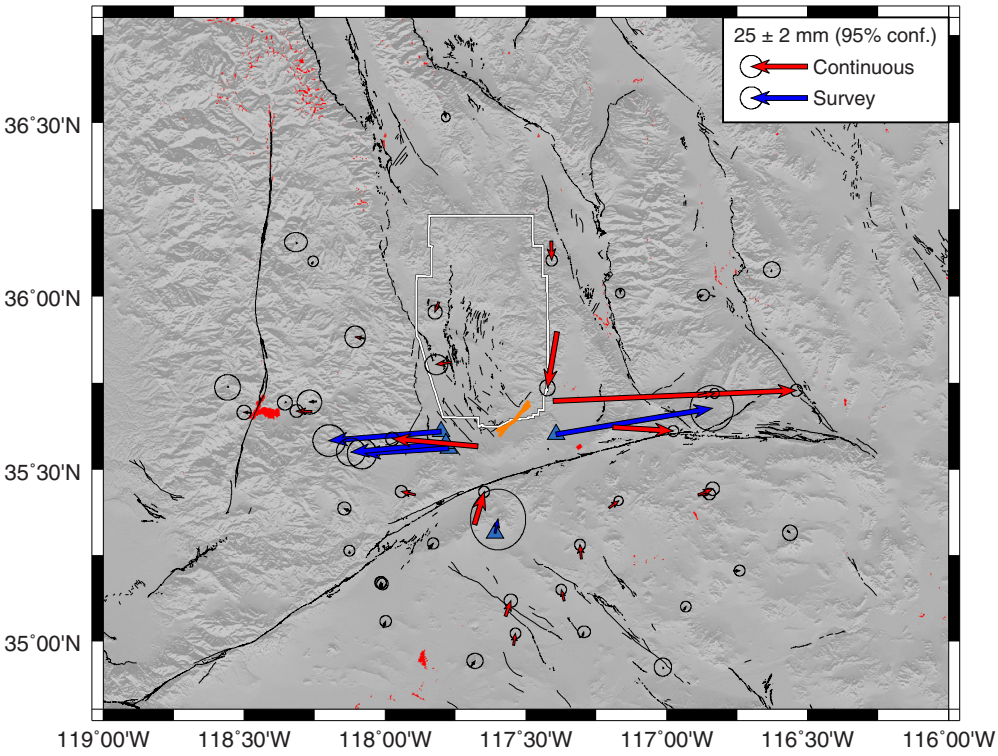

Figure 2. Displacements of the 4 July 2019 M_w 6.4 Ridgecrest earthquake. Red vectors are for continuous sites and blue are for survey sites (four University of California, Riverside [UCR] installed within hours of the first earthquake). Light blue triangles show the five survey sites occupied by UCR after the M_w 6.4 earthquake and hence during the M_w 7.1 earthquake. The surface rupture is marked by the orange line (C. Milliner, personal comm., 2019, via SCEC Response Forum; see Data and Resources), and the white line is the boundary of the NAWS China Lake, as in Figure 1. Displacements shown are listed in Table S1. The color version of this figure is available only in the electronic edition.

In the days that followed the two events, multiple additional sites were occupied in the epicentral region by groups from Scripps Institution of Oceanography (SIO) at the University of California, San Diego (UCSD), the Nevada Geodetic Laboratory (NGL) at the University of Nevada, Reno (UNR), and the USGS, as well as by UCR. Coordination among these groups enabled an efficient field response, maximizing coverage while minimizing duplication of effort. Given the difficulties of obtaining access to the Naval Air Weapons Station (NAWS) China Lake (see Fig. 1), within which the majority of the surface ruptures occurred, the effort from UCR, SIO/UCSD, and NGL/UNR focused on the area outside of the NAWS, leaving the responsibility of occupying sites within the NAWS to the USGS (B. A. Brooks *et al.*, unpublished manuscript, 2019; see Data and Resources). By the end of 9 July, local time, 20 survey sites had been occupied by UCR (light blue triangles in Figs. 2–4), SIO/UCSD (gold triangles in Figs. 3 and 4), and NGL/UNR (purple triangles in Figs. 3 and 4) combined, and a further 13 sites, including eight stations forming four cross-fault arrays targeted at detecting shallow afterslips, had been installed by the USGS. Some of the monuments are metal rods cemented into competent rocks, occupied by a GNSS antenna mounted on a tripod; others involve a concrete block with a threaded metal rod on which an antenna could be attached directly, without the need for a tripod (see Fig. S3 for several examples). Each of the survey sites recorded data at a standard low rate (e.g., 15 or 30 s) for daily processing, using an Ashtech Z-12, Septentrio PolaRx5, Topcon GB-1000 or Trimble R7, NetRS or NetR9 receiver with an Ashtech Choke Ring, Topcon PG-A1 or Trimble Geodetic L1/L2 Compact, Zephyr Geodetic or Zephyr Geodetic 2 antenna.

With additional deployments in the days and weeks that followed, by 7 September 27 sites had been occupied by UCR, SIO/UCSD, and NGL/UNR, and a further 16 by the USGS, the majority of these in a "semicontinuous" mode (e.g., Blewitt *et al.*, 2009), whereby the stations are powered to run for weeks at a time and infrequently serviced to retrieve data, check the centering of antennas, and perform maintenance. The majority of these semicontinuous stations will be operated into 2020 to capture details of any postseismic transient motion following the earthquakes. High-rate data during the earthquakes themselves are available for most of the continuous sites in the region operated by UNAVCO (G. S. Mattioli *et al.*, unpublished manuscript, 2019; see Data and Resources; UNAVCO Community, 2019).

GNSS Processing

The solutions were processed using a prerelease version of GAMIT/GLOBK 10.71 (update of Herring, King, *et al.*, 2018). The results of the surveys were then combined with processed solutions for NOTA continuous sites within the surrounding region. These solutions differ slightly from the official GAGE solutions in that they were split on the days of the earthquakes to avoid artifacts in the time series; the usual 00:00 GPST (GPS Time) to 00:00 GPST processing day straddles a major displacement, resulting in a time-series points that lies at a weighted average between the positions before and after the earthquake on the day of the event itself.

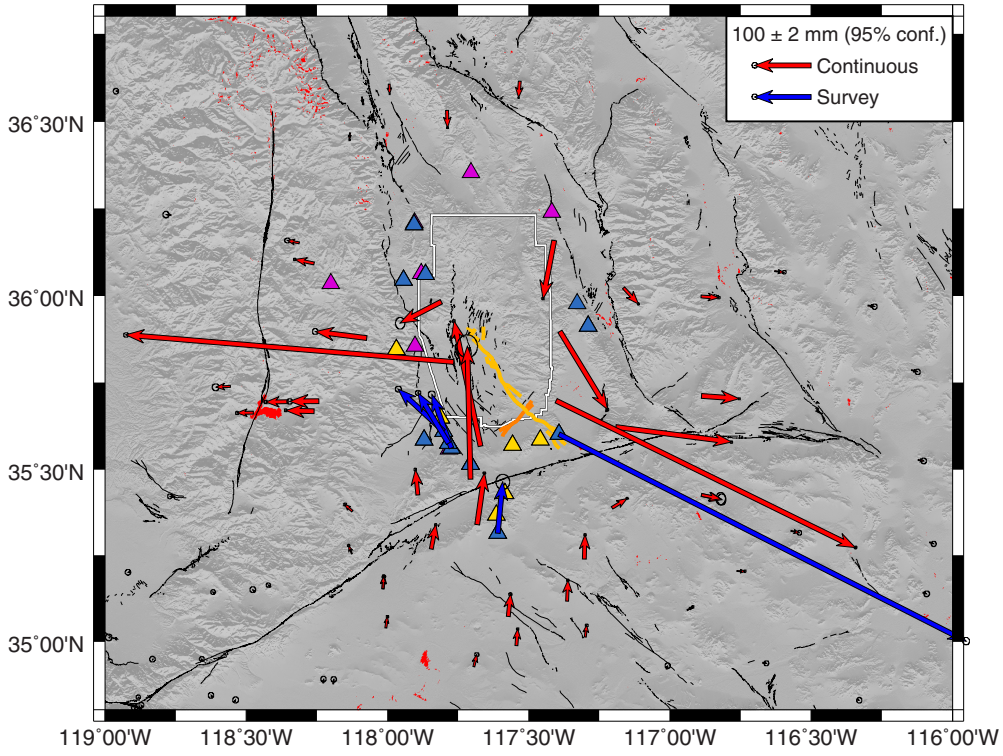

Figure 3. Displacements of the 6 July (5 local time) 2019 M_w 7.1 Ridgecrest earthquake. Vector colors and fault rupture for the first earthquake are as in Figure 2, with the M_w 7.1 rupture in light orange. Gold triangles are sites occupied by Scripps Institution of Oceanography/University of California, San Diego after the M_w 7.1 earthquake and therefore do not have coseismic displacement estimates for the second earthquake separately from the first; purple triangles are semicontinuous sites occupied by Nevada Geodetic Laboratory/University of Nevada, Reno. Displacements shown are listed in Table S2. The color version of this figure is available only in the electronic edition.

The data from the continuously running GNSS receivers in the region were processed for the period between 2 July (day 183) and 9 July (day 190), 2019, in nominally 24 hr sessions. On the days of the earthquakes, the 24 hr sessions were divided into two sessions. The first session ran from 00:00 GPST to the minute before the earthquake on that day, and the second session started 5 min after the earthquake origin time and finished at 23:59:30 GPST. The processing was carried out in eight subnetworks each containing 66–67 stations. The 507 stations processed spanned a region about twice the diameter of the area likely to have undergone more than 1 mm of the coseismic displacement from the 6 July M_w 7.1 event. The satellite orbits were fixed to the International GNSS Service global orbits. The division of the networks and the processing of the data followed that same approach described for the GAMIT processing in Herring *et al.* (2016). The realization of the reference frame was the same as that described in Herring *et al.* (2016), but the newer North America 2014 (NAM14) was used. The positions, velocities, and reference frame sites for NAM14 are available from UNAVCO (see Data and Resources).

The data from the survey sites (five light blue triangles in Figs. 2–4) that were set up from 5 July (day 186) onward (see Fig. S2) captured the second earthquake. These sites were processed in one session for the 27 hr between their deployment and the second earthquake at 03:12 UTC on 6 July 2019 (day 187), for the 21 hr remaining after the earthquake on 6 July 2019, and for standard 24 hr UTC-day sessions thereafter. These results were then combined with the similarly arranged sessions from the processing of the continuous sites.

Four of the survey sites had been measured previously during the February and March 2019 surveys (Funning, Terry, and Floyd, 2019; see the Previous Surveys and Velocity Solutions section), but the sites did not have enough previous data to determine a velocity before the earthquake. We therefore assumed, in the four to five months between their first observation and the first earthquake (Funning, Kyriakopoulos, *et al.*, 2019), motion consistent with a velocity constrained to within 0.5 mm/yr of nearby continuous site RAMT for survey site ATOL; of the mean velocity of nearby continuous sites CCCC and P616, which have velocities within 1 mm/yr of each other, for survey sites F048, H701, and J701; and of the mean velocity of nearby continuous sites CCCC, P580, and P595 for survey site PNCL. This allowed us to estimate displacements at these sites during the first earthquake. Furthermore, we similarly constrained the pre-earthquake velocity for a few survey sites with imprecise estimates due to short or few previous observations: 0806 was constrained in the same way as ATOL; survey site INYO in the same way as F048, H701 and J701; and V511 to the velocity of nearby survey site BM25. This allowed us to estimate cumulative displacements at these sites due to both earthquakes combined, having been observed again only after the second earthquake.

We processed all data from previous surveys that contained data from sites occupied in the aftermath of the earthquakes (see Table S1). We also include the results from McClusky *et al.* (2001) by incorporating their full solution and associated covariance matrix in the combination of the survey and one-week continuous results.

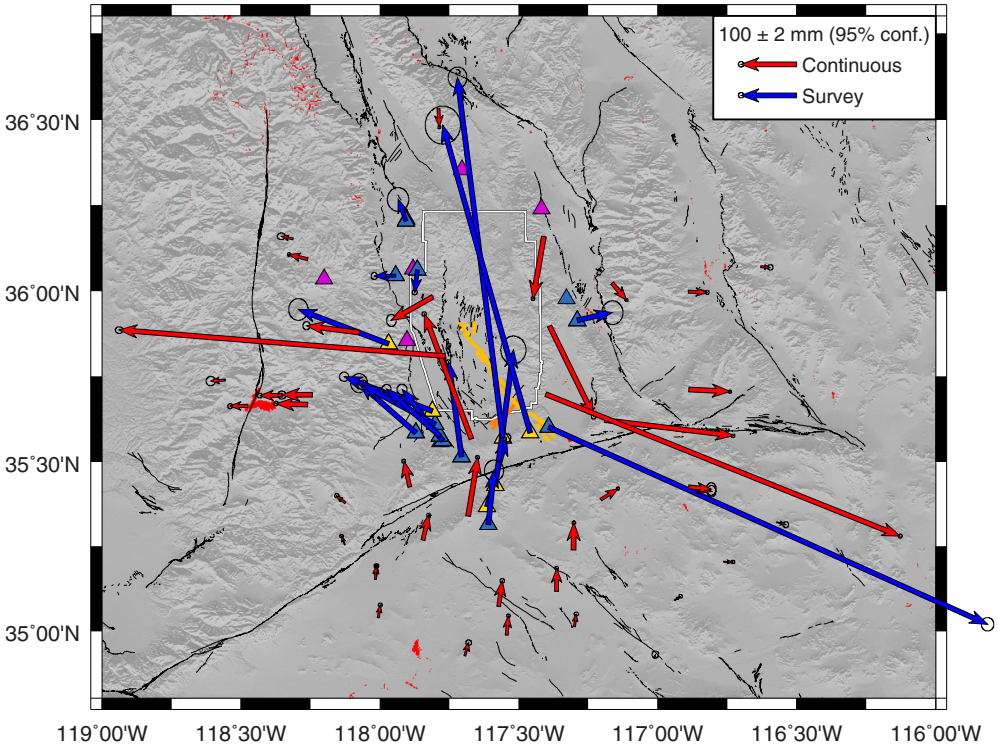

Figure 4. Cumulative displacements from the two earthquakes combined. Vector colors and fault ruptures are as in Figure 3. Displacements shown are listed in Table S3. The color version of this figure is available only in the electronic edition.

Results

Figures 2–4 show the estimated displacements after combining the continuous and survey solutions described in the GNSS Processing section, for the first M_w 6.4 earthquake, the second M_w 7.1 earthquake, and the two earthquakes combined, respectively. Unfortunately, many of the sites occupied immediately after the earthquakes (triangles in Figs. 3 and 4) do not have sufficient data from before the earthquakes to allow reasonable estimation of coseismic displacements from prior observations alone. Many of them were last measured briefly around the time of the 1999 Hector Mine earthquake, and therefore are subject to not only a long period (20 yr) of no observations but also short, segmented time series and perturbed tectonic velocities, both leading to poorly constrained pre-earthquake velocities. Nevertheless, we explain our approach to constraining their pre-earthquake velocities, and therefore coseismic displacements, in GNSS Processing section.

Four survey sites to the west and south of the first M_w 6.4 earthquake help constrain the displacements in a region where only two nearby continuous sites otherwise exist in the near field (Fig. 3). The same four survey sites help constrain the southern west side of the second M_w 7.1 earthquake, as well as PNCL at the very southern end of the rupture.

The displacements for the M_w 6.4 earthquake (Fig. 2) are consistent with a predominantly left-lateral rupture, as we observed in the immediate aftermath of the earthquake. The closest sites to the rupture show displacements of 3 and 11 cm (at H701 and P595, respectively) that are oriented oblique to the strike of the fault, a consequence of their locations beyond the ends of the rupture and in keeping with the expected deformation pattern for a finite left-lateral strike-slip fault. For the M_w 7.1 earthquake (Fig. 3), we observe a clear right-lateral displacement pattern overall, consistent with the northwest strike of the mapped ruptures in the area, with fault-parallel displacements at sites located within a zone perpendicular to the major surface rupture and rotation of the displacement vectors at sites beyond the ends of the rupture. The largest recorded displacements of ~80 cm are at survey site PNCL, with a trend that is subparallel to the local fault strike.

Summary

We present a coseismic displacement solution for combined continuous and survey GNSS, for both the M_w 6.4 and M_w 7.1 July 2019 Ridgecrest earthquakes separately and combined. To obtain these results, we reprocessed previous surveys from the 1990s and 2000s, as well as presenting more recent surveys from February and March 2019 to the west and south of the Ridgecrest ruptures. These results help constrain particularly the separate ground displacements, as well as eventually the continuing postearthquake motions, if any, after more observations continue to be made at the same GNSS sites. All postearthquake survey data collected by UCR and SIO/UCSD are archived at UNAVCO, which will be supplemented as further surveys are conducted.

We recommend that, for the purposes of earthquake response, GNSS surveys remain a vital component of geodetic observations that should be undertaken regularly to avoid long gaps in time series, which decrease the precision of eventual pre-earthquake positions and may also be contaminated by otherwise unobserved nonsecular velocity perturbations. We also suggest that the processed solutions (e.g., Solution Independent Exchange format; SINEX) for previous surveys be made readily available, in addition to the raw (e.g., Receiver-Independent Exchange format; RINEX) data currently archived on a routine basis by working groups. When the need for rapid response

arises, well-informed field teams are required to target sites that are likely to produce the best coseismic and postearthquake measurements. Furthermore, we recommend that postearthquake surveys are conducted at high rates of observation (i.e., greater than 1 Hz frequency) for potential seismogeodetic studies in the case of large aftershocks or, as in the case of the Ridgecrest earthquakes, a larger secondary earthquake, although such an approach does proportionally increase the burden of regular recovery of data on field teams to conserve receiver disk storage.

Data and Resources

Table 1 contains a list of surveys processed for this work, each of which are available from UNAVCO via the digital object identifiers (DOIs) in the final column. Additional Receiver-Independent Exchange (RINEX) files processed for this work are available from the U.S. Geological Survey (USGS) via the Northern California Earthquake Data Center (NCEDC; ftp://ftp.ncedc.org/pub/gps/survey/usgs/) and from Southern California Earthquake Center (SCEC) via the Southern California Earthquake Data Center (SCEDC; https://service.scedc.caltech.edu/gps/). GAGE position and velocity solutions in the NAM14 reference frame are available at ftp://data-out.unavco.org/pub/products/velocity/pbo.final_nam14.vel. The surface ruptures plotted in Figs. 2–4 are available from the SCEC Response Forum at https://response.scec.org/. All websites were last accessed in December 2019. Additional information is from the following unpublished manuscripts: B. A. Brooks, J. Murray, J. Svarc, E. Phillips, R. Turner, M. Murray, T. Ericksen, K. Wang, S. E. Minson, R. Burgmann, F. Pollitz, K. Hudnut, E. A. Roeloffs, J. Hernandez, and B. Olson, 2019, *Rapid geodetic observations of spatiotemporally varying postseismic deformation following the Ridgecrest earthquake sequence: The US Geological Survey response*; and G. S. Mattioli, D. A. Phillips, K. M. Hodgkinson, C. Walls, D. J. Mencin, B. A. Bartel, D. J. Charlevoix, C. Crosby, M. J. Gottlieb, B. Henderson, W. Johnson, D. Maggert, D. Mann, C. M. Meertens, J. Normandeau, J. Pettit, C. M. Puskas, L. Rowan, C. Sievers, and A. Zaino, 2019, *The GAGE data and field response to the 2019 Ridgecrest earthquake sequence*. Supplemental material for this article includes Table S1, containing the coseismic displacements estimated due to the first M_w 6.4 earthquake, shown in Figure 2; Table S2, containing the coseismic displacements estimated due to the second M_w 7.1 earthquake, shown in Figure 3; Table S3, containing the cumulative coseismic displacements estimated due to both earthquakes combined, shown in Figure 4; and three figures showing the return of data from the February and March 2019 surveys described in the main article (Fig. S1), a summary of survey sites observed within six days and 40 km of the July 2019 earthquakes (Fig. S2), and photographs of several types of geodetic monuments used during these surveys (Fig. S3).

Acknowledgments

This article is dedicated to Meghan M. Miller, on her retirement as President of UNAVCO, upon whose foresight and data collection this study is built.

Keith Richards-Dinger, Baoning Wu, Christos Kyriakopolous, Jordan Cortez, John Conrad, Lisa Knowles, and Filiz Duda are thanked for assistance in the field. Duncan Agnew is thanked for his timely advice on possible survey targets in the aftermath of the earthquakes. The authors also thank Ronni Grapenthin and Tony Lowry for their reviews, which greatly improved the article. This material is based on services provided by the Geodesy Advancing Geoscience and EarthScope (GAGE) Facility, operated by UNAVCO, Inc., with support from the National Science Foundation (NSF) and the National Aeronautics and Space Administration under NSF Cooperative Agreement EAR-1724794. This research was supported by the Southern California Earthquake Center (SCEC; Contribution Number 9995), Awards 14189 (Funning), 18201 (Funning and Terry), and 19106 (Floyd); and by NSF Rapid Response Research (RAPID) program Awards 1945728 (Funning) and 1945760 (Fialko). SCEC is funded by NSF Cooperative Agreement EAR-1600087 and USGS Cooperative Agreement G17AC00047. This is SCEC Contribution Number 9995.

References

Altamimi, Z., L. Métivier, P. Rebischung, H. Rouby, and X. Collilieux (2017). ITRF2014 plate motion model, *Geophys. J. Int.* **209,** 1906–1912, doi: 10.1093/gji/ggx136.

Bevis, M., and K. Hudnut (2005a). *GeoEarthScope ALS San Andreas Fault (B4)—2005-B4-Phase 1*, UNAVCO, Inc., GPS/GNSS Observations Dataset, doi: 10.7283/V5MV-QE58.

Bevis, M., and K. Hudnut (2005b). *GeoEarthScope ALS San Andreas Fault (B4) - 2005-B4-Phase 2*, UNAVCO, Inc., GPS/GNSS Observations Dataset, doi: 10.7283/FQ3X-X311.

Blewitt, G., W. C. Hammond, and C. Kreemer (2009). Geodetic observation of contemporary deformation in the northern Walker Lane: 1. Semipermanent GPS strategy, in *Late Cenozoic Structure and Evolution of the Great Basin-Sierra Nevada Transition*, J. S. Oldow and P. H. Cashman (Editors), Special Paper 447, Geological Society of America (GSA), Boulder, Colorado.

Fialko, Y., and M. Simons (2000). Deformation and seismicity in the Coso geothermal area, Inyo County, California: Observations and modeling using satellite radar interferometry, *J. Geophys. Res.* **105,** 21,781–21,794, doi: 10.1029/2000JB900169.

Fialko, Y., Z. Jin, E. Tymofyeyeva, D. T. Sandwell, J. Haase, and M. A. Floyd (2019a). *Ridgecrest California Earthquake Response 2019*, UNAVCO, Inc., GPS/GNSS Observations Dataset, doi: 10.7283/N74Q-GA66.

Fialko, Y, Z. Jin, E. Tymofyeyeva, D. T. Sandwell, J. Haase, and M. A. Floyd (2019b). *Ridgecrest California Earthquake Post-Event Response July 2019 UCSD*, UNAVCO, Inc., GPS/GNSS Observations Dataset, doi: 10.7283/YJK0-B215.

Funning, G. (2016). *San Jacinto Fault 2014*, UNAVCO, Inc., GPS/GNSS Observations Dataset, doi: 10.7283/T57H1GZW.

Funning, G., C. Kyriakopoulos, B. Wu, K. Richards-Dinger, J. Cortez, and M. A. Floyd (2019). *Ridgecrest California Earthquake Response 2019*, UNAVCO, Inc., GPS/GNSS Observations Dataset, doi: 10.7283/5ASB-9V26.

Funning, G., R. Terry, and M. A. Floyd (2019). *SCEC Mojave 2019*, UNAVCO, Inc., GPS/GNSS Observations Dataset, doi: 10.7283/TFX5-EJ21.

Herring, T. A., M. A. Floyd, and R. W. King (2018). *GAGE Processing GPS Plate Boundary Observatory Expanded Analysis Product for 2017: Final (Annual) Velocity Field; Combination in Nab08 (IGb08 Rotated into the North America Frame) Reference Frame Using Kalman Filter Analysis of SINEX files from CWU, NMT*

and PBO Produced by the Massachusetts Institute of Technology (Analysis Center Coordinator), UNAVCO, Inc., GPS/GNSS-Based Geodetic Derived Data Product, doi: 10.7283/P2GT0N.

Herring, T. A., R. W. King, M. A. Floyd, and S. C. McClusky (2018). *Introduction to GAMIT/GLOBK, Release 10.7*, Massachusetts Institute of Technology, Cambridge, Massachusetts, available at http://geoweb.mit.edu/gg/Intro_GG.pdf (last accessed December 2019).

Herring, T. A., T. I. Melbourne, M. H. Murray, M. A. Floyd, W. M. Szeliga, R. W. King, D. A. Phillips, C. M. Puskas, M. Santillan, and L. Wang (2016). Plate Boundary Observatory and related networks: GPS data analysis methods and geodetic products, *Rev. Geophys.* **54,** 759–808, doi: 10.1002/2016RG000529.

McClusky, S. C., S. C. Bjomstad, B. H. Hager, R. W. King, B. J. Meade, M. M. Miller, F. C. Monastero, and B. J. Souter (2001). Present day kinematics of the Eastern California Shear Zone from a geodetically constrained block model, *Geophys. Res. Lett.* **28,** 3369–3372, doi: 10.1029/2001GL013091.

Miller, M. M., and D. J. Johnson (2001a). *Mojave 1999*, UNAVCO, Inc., GPS/GNSS Observations Dataset, doi: 10.7283/T56Q1V5W.

Miller, M. M., and D. J. Johnson (2001b). *Mojave 2000*, UNAVCO, Inc., GPS/GNSS Observations Dataset, doi: 10.7283/T5JW8BS7.

Miller, M. M., and D. J. Johnson (2001c). *Garlock 2000*, UNAVCO, Inc., GPS/GNSS Observations Dataset, doi: 10.7283/T5KW5CXM.

Miller, M. M., and D. J. Johnson (2001d). *Mojave 2001 03 (Mar)*, UNAVCO, Inc., GPS/GNSS Observations Dataset, doi: 10.7283/T5Z60KZ5.

Miller, M. M., and D. J. Johnson (2001e). *Garlock 2001 03 (Mar)*, UNAVCO, Inc., GPS/GNSS Observations Dataset, doi: 10.7283/T5TD9V79.

Miller, M. M., and D. J. Johnson (2001f). *Mojave 2001 06 (Jun)*, UNAVCO, Inc., GPS/GNSS Observations Dataset, doi: 10.7283/T5F769GJ.

Miller, M. M., and D. J. Johnson (2001g). *Garlock 2001 06 (Jun)*, UNAVCO, Inc., GPS/GNSS Observations Dataset, doi: 10.7283/T5G44N6M.

Miller, M. M., M. P. Golombek, and R. K. Dokka (1997). *Mammoth/Mojave 1994*, UNAVCO, Inc., GPS/GNSS Observations (Aggregation of Multiple Datasets), doi: 10.7283/T57H1GGM.

Miller, M. M., E. Humphreys, R. K. Dokka, and F. H. Webb (1995). *Mojave 1995*, UNAVCO, Inc., GPS/GNSS Observations Dataset, doi: 10.7283/T5H12ZX8.

Miller, M. M., E. Humphreys, R. K. Dokka, and F. H. Webb (2001a). *Garlock 1997*, UNAVCO, Inc., GPS/GNSS Observations Dataset, doi: 10.7283/T55Q4T1H.

Miller, M. M., E. Humphreys, R. K. Dokka, and F. H. Webb (2001b). *Mojave 1997*, UNAVCO, Inc., GPS/GNSS Observations Dataset, doi: 10.7283/T5W66HPD.

Miller, M. M., E. Humphreys, R. K. Dokka, and F. H. Webb (2001c). *Garlock 1998 06 (Jun)*, UNAVCO, Inc., GPS/GNSS Observations Dataset, doi: 10.7283/T51Z4295.

Miller, M. M., E. Humphreys, R. K. Dokka, and F. H. Webb (2001d). *Mojave 1998 06 (Jun)*, UNAVCO, Inc., GPS/GNSS Observations Dataset, doi: 10.7283/T58G8HMF.

Miller, M. M., E. Humphreys, R. K. Dokka, and F. H. Webb (2001e). *Mojave 1998 12 (Dec)*, UNAVCO, Inc., GPS/GNSS Observations Dataset, doi: 10.7283/T50Z715S.

Miller, M. M., E. Humphreys, R. K. Dokka, and F. H. Webb (2001f). *Garlock 1998/1999*, UNAVCO, Inc., GPS/GNSS Observations Dataset, doi: 10.7283/T59G5JRT.

Miller, M. M., D. J. Johnson, T. H. Dixon, and R. K. Dokka (2001). Refined kinematics of the Eastern California shear zone from GPS observations, 1993-1998, *J. Geophys. Res.* **106,** 2254–2263, doi: 10.1029/2000JB900328.

Shen, Z.-K., R. W. King, D. C. Agnew, M. Wang, T. A. Herring, D. Dong, and P. Fang (2011). A unified analysis of crustal motion in Southern California, 1970–2004: The SCEC crustal motion map, *J. Geophys. Res.* **116,** no. B11402, doi: 10.1029/2011JB008549.

Tymofyeyeva, E., and Y. Fialko (2015). Mitigation of atmospheric phase delays in InSAR data, with application to the Eastern California Shear Zone, *J. Geophys. Res.* **120,** 5952–5963, doi: 10.1002/2015JB011886.

UNAVCO Community (2019). *Ridgecrest California Earthquake Response 2019: Network of the Americas (NOTA) High Rate GNSS Data*, UNAVCO, Inc., GPS/GNSS Observations (Aggregation of Multiple Datasets), doi: 10.7283/HZN1-5910.

U.S. Geological Survey and California Geological Survey (2006). Quaternary fault and fold database for the United States, available at USGS website https://earthquake.usgs.gov/hazards/qfaults/ (last accessed June 2019).

Wang, K., and R. Bürgmann (2019). Coseismic and early postseismic deformation due to the 2019 Ridgecrest earthquake sequence constrained by Sentinel-1 and COSMO-SkyMed SAR data, *Seismol. Res. Lett.* **91,** doi: 10.1785/0220190299.

Xu, X., and D. Sandwell (2019). Coseismic displacements and surface fractures from Sentinel-1 InSAR: 2019 Ridgecrest earthquakes, *Seismol. Res. Lett.* **91,** doi: 10.1785/0220190275.

Manuscript received 22 October 2019
Published online 12 February 2020